Pairwise Orthogonal Transform for Spectral Image Coding

Ian Blanes, *Student Member, IEEE,* and Joan Serra-Sagristà, *Member, IEEE*

***Abstract*—Spectral transforms are widely used for the codification of remote-sensing imagery, the KLT and wavelets being the two most common transforms. The KLT presents a higher coding performance than wavelets; however, it also carries several disadvantages: high computational cost and memory requirements, a difficult implementation, and its lack of scalability. In this paper, we introduce a novel transform based on the KLT that, while obtaining better coding performance than wavelets, does not have the mentioned disadvantages of the KLT. Due to its very small amount of side-information, the transform can be applied in a line-based scheme, which specially reduces the transform memory requirements. Extensive experimental results are conducted for AVIRIS and Hyperion images, both for lossy and lossless, and in combination with various hyperspectral coders. Results for effects on RX anomaly detection and k-means clustering are also included. Theoretical and experimental evidence suggest that the proposed transform might be good replacement for wavelets as spectral decorrelator in many of the situations where the KLT is not a suitable option.**

***Index Terms*—Hyperspectral image coding, Karhunen-Loêve Transform (KLT), embedded systems, memory-constrained environments, progressive lossy-to-lossless (PLL) and lossy compression.**

I. Introduction

SPECTRAL transforms are receiving much attention in several applications of the remote sensing field, for instance in dimensionality reduction for classification or monitoring purposes. However, spectral transforms are particularly relevant in hyperspectral image compression, because of the high spectral redundancy among components, which, when exploited, yields substantial coding gains [1], thus improving storage and transmission capabilities.

The most common spectral transforms in hyperspectral image coding are wavelet transforms and the Karhunen-Loêve Transform (KLT). The KLT produces more competitive coding results, as it is trained for each input image to provide optimal decorrelation. Nonetheless, several significant disadvantages have been identified for the KLT: an extremely high computational cost and memory requirement, its higher implementation difficulty, and that it is not a scalable transform, impairing component scalability. These disadvantages restrain the use of the KLT in several situations, such as in interactive or real-time processing, and in power or memory-constrained environments like on-board sensors. Wavelets, on the other hand, lack the superior coding gains of the KLT, but have much lower computational costs and memory requirements, which are compatible with the resource-constrained scenarios described before. In addition, they also provide component scalability.

The particularities of two scenarios where a hyperspectral transform coder might be used are worth discussing in detail. When a transform coder is used on-board a plane or a spacecraft, an image coder has to process uncalibrated information that might have varying features if compared with calibrated versions of the same information, such as for example echo, smear or streaking artifacts [2]. In this first scenario, important features of a coder are to have low forward computational and memory costs, and, if bandwidth from the sensor is limited, to be able to operate in lossy or Progressive Lossy-to-Lossless (PLL) mode. In a second scenario, document retrieval from an archive, important features are coding gains for both lossy and lossless, but also PLL operation, high component scalability, and acceptable computational costs for decoding.

When analyzing the origins of the four cited disadvantages of the KLT, we note that two of them —high computational cost, and not being a scalable transform— are direct consequences of its optimal decorrelation property, which requires all of the transform inputs to be present in the calculation of each output. The third disadvantage —a high memory requirement— is caused by the two sequential stages of the forward transform, i.e., the whole image is first inspected during a training stage, and then processed for a second time for the transform application. And the fourth disadvantage —higher implementation difficulty— is due to the difficulties posed by the iterative numerical algorithm commonly used in the last part of the training stage.

To overcome the high computational cost, the Discrete Cosine Transform (DCT) was proposed [3], which assumes a Toeplitz matrix as data covariance matrix; however, the DCT has a poor performance as spectral decorrelator [4]. Similar approaches to reduce the computational cost are the fast Approximate Karhunen-Loêve Transform (AKLT) [5] and the AKLT_2 [6], which extend the DCT with first and second order perturbations.

If the spatial size of an image is large enough, transform training costs, which amount to one fifth of the total computational cost, can be reduced as proposed in [4]. The proposal is based on the extrapolation of the empirical covariance matrix from a small sample of the whole input, and is shown to be effective with very small sampling factors. On the other hand if the spatial size of an image is significantly small or if the transform is applied in multiple spatial blocks, then Eigenvalue Decomposition (ED) costs are more significant and methods

This work was supported in part by the Spanish Government, by the Catalan Government, and by FEDER under grants TIN2009-14426-C02-01, TIN2009-05737-E/TIN, SGR2009-1224, and FPU2008. Computational resources used in this work were partially provided by the Oliba Project of the Universitat Autònoma de Barcelona.

such as [7] might reduce them. Training costs can also be diminished by pretraining a transform for a generic set of images [8], [9]. Pretraining has the drawback that it produces inferior coding gains because of the lack of specificity.

Two further improvements to the KLT are also worth pointing out: first, for lossless coding, a method is proposed to replace multiplication operations in the application and removal stages of the transform by incorporating them into the lifting decomposition [10], [11], and thus applying a transform with only addition and shift operations; second, coding gains can be improved by not assuming Gaussian sources, and finding the Optimal Spectral Transform with an ICA-based algorithm [12], [13], which can also be pretrained [14], [15].

In addition, to overcome the high computational cost and the lack of component scalability disadvantages of the KLT, a few recent papers propose to use a divide-and-conquer approach in the transform application to achieve substantial gains in computational costs and reasonable scalability, and still obtain a virtually equal coding performance. In [16], computational costs are reduced for lossless compression of magnetic resonance images by using a recursively clustered KLT. Similarly, we developed a multilevel clustered KLT structure for PLL coding [17]. This structure yields greater savings, and leads to the family of structures discussed in [18], which have reduced costs and better scalability. Other divide-and-conquer approaches are [19], [20], where two levels of clusters are applied, and [21], where a single-level clustering is used to reduce the amount of side information and improve transform performance on low bitrates for images with a small spatial size. Nonetheless, all previous divide-and-conquer approaches still present difficult implementations and memory requirements of the order of those of the KLT.

In this paper, we employ a divide-and-conquer strategy to propose a very simple transform that requires a very small amount of side information, which in its turn allows for a line-based application of the transform not previously available to other divide-and-conquer approaches. As will be shown, the proposed transform still has very good coding performance —better than wavelet transforms—, and is capable of overcoming all the four related inconveniences of the KLT, achieving notably lower computational costs and better component scalability, and particularly with a very low memory requirement.

This paper is organized as follows. Section II introduces the proposed pairwise orthogonal transform. Section III contains the experimental results. Section IV draws some conclusions.

II. Pairwise Orthogonal Transform

This section introduces first the proposed simple spectral transform for hyperspectral image coding, then it considers some implementation issues, and finally it provides an analytical evaluation of its properties.

A. Transform Definition

The proposed transform is based on the application of a divide-and-conquer strategy to the KLT, where the resulting transform is a composition of smaller KLT transforms, namely, a composition of KLTs for only two image components each.

In a full KLT, all components are decorrelated with each other, independently of how much energy they share, i.e., independently of how high is their covariance. On the contrary, the proposed Pairwise Orthogonal Transform (POT) has a structure that decorrelates parts with high shared energy, while ignoring the other parts, as parts with low energies have lower influence in the coding performance.

A POT is organized in multiple levels. In the first level, a two-component KLT transform is applied to every pair of consecutive components, and the same approach is repeated in successive levels, but, at each level, only further decorrelating the first resulting component of each transform of the previous level. To clarify, the structure of a POT for eight components is shown in Fig. 1. In case of unpaired components, which occurs if the number of components in one level is an odd number, the unpaired component is directly forwarded to the next level; unpaired components are alternatively selected from the left and right hand sides at successive levels.

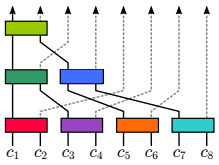

Figure 1. Proposed pairwise structure for an image of eight components, where each rectangle corresponds to a two-component KLT.

With the proposed structure, as with the KLT, most of the image energy is accumulated in the first components, since each of the two-component KLTs operates as a classic KLT, grouping most of the signal energy in one of the two resulting components —the principal component—, and hence allowing most of the energy to flow across the composition of transforms up to the resulting components of the last levels. Moreover, the combination of multiple KLT instances produces also an orthogonal transform, which still preserves image variance across domains, and allows for direct distortion estimation on the transformed domain.

Let us recall the definition of a classic N component KLT: let X be a matrix that has N rows, one for each source, and M columns, one for each sample. Then, Y, the outcome after applying the transform, is computed as

$$Y = \mathrm{KLT}_{\Sigma_X}(X) = Q^T X, \tag{1}$$

where $\Sigma_X = (1/M)XX^T$ is the covariance matrix of X, and Q is the orthogonal matrix obtained from the ED of $\Sigma_X = Q\Lambda Q^{-1}$ ($\Lambda = diag(\lambda_1, \ldots, \lambda_N)$, $|\lambda_1| \geq |\lambda_2| \geq \ldots \geq |\lambda_N|$). Note that sources must be manually centered around zero if they do not have zero mean. The covariance matrix of Y is the diagonal matrix Λ, and $\lambda_1, \ldots, \lambda_N$ are the variances of each component after the transform.

With the use of only two-component KLTs, the ED procedure is greatly simplified, overcoming one of the previously described KLT inconveniences, the implementation difficulty. The following is a numerically stable solution, that does not

require any iterative process to obtain Q:

$$Q = \begin{pmatrix} p & q \\ t & u \end{pmatrix}, \Lambda = \begin{pmatrix} \lambda_1 & 0 \\ 0 & \lambda_2 \end{pmatrix},$$

where

$$t = -q = \frac{b}{|b|}\sqrt{\frac{1}{2} - \frac{(a-d)}{2s}},$$

$$p = u = \sqrt{\frac{1}{2} + \frac{(a-d)}{2s}} = \sqrt{1-t^2}, \quad (2)$$

$$\lambda_1 = \frac{a+d+s}{2}, \lambda_2 = \frac{a+d-s}{2},$$

$$s = \sqrt{(a-d)^2 + 4b^2},$$

and

$$\Sigma_{\mathrm{X}} = \begin{pmatrix} a & b \\ b & d \end{pmatrix}.$$

While computing Q, two precautions have to be taken into account. First, if $b = 0$, then t and q are undefined; however, assuming $\frac{b}{|b|}$ to be either 1 or -1 is a sufficient solution. Second, $s \simeq 0$ if inputs are similar and share almost no energy, which causes a division by zero. An appropriate remedy is to use an identity matrix as Q.

Likewise, the same reasoning can also be extended to the lifting decomposition of a two-component transform, which allows the transform to be applied in a lossless mode. The lifting decomposition and application of the KLT, otherwise known as Reversible KLT (RKLT) is performed as described either in [22] or in [23]. The RKLT is based on decomposing a transform matrix into multiple elementary matrices, each one equivalent to a sequence of lifting steps, and then perform the matrix multiplication by using these lifting sequences. For a two-component transform, regardless of which of the two methods are used, the required sequence of elementary matrices is of this form:

$$Q^T = \begin{pmatrix} p & t \\ q & u \end{pmatrix} = \begin{pmatrix} 1 & 0 \\ 0 & s \end{pmatrix} P \begin{pmatrix} 1 & 0 \\ w_3 & 1 \end{pmatrix} \begin{pmatrix} 1 & w_2 \\ 0 & 1 \end{pmatrix} \begin{pmatrix} 1 & 0 \\ w_1 & 1 \end{pmatrix}.$$

The following is a solution for the previous equation,

$$\begin{cases} P = \left(\begin{smallmatrix} 1 & 0 \\ 0 & 1 \end{smallmatrix}\right), w_1 = w_3 = \frac{p-1}{t}, \\ w_2 = t, s = \mathrm{Det}(Q) \end{cases} \text{for } |t| \geq |p|,$$

$$\begin{cases} P = \left(\begin{smallmatrix} 0 & 1 \\ 1 & 0 \end{smallmatrix}\right), w_1 = w_3 = \frac{1-t}{p}, \\ w_2 = -p, s = -\mathrm{Det}(Q) \end{cases} \text{for } |t| < |p|.$$

As Q is orthogonal, $t^2 + p^2 = 1$, therefore, the condition $|t| \geq |p|$ is enough to guarantee that no division by zero occurs. Note that s only affects the sign of the non-principal result, which is not further transformed, and as changing the sign of an entire component is usually irrelevant to hyperspectral encoders, it can always be assumed to be positive. The associated lifting structure to perform $\left(\begin{smallmatrix} y_1 \\ y_2 \end{smallmatrix}\right) = Q^T \left(\begin{smallmatrix} x_1 \\ x_2 \end{smallmatrix}\right)$, as shown in Fig. 2, requires only 9 operations and a conditional permutation.

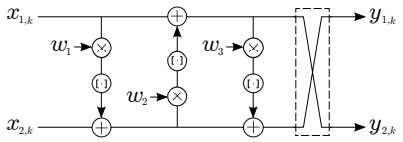

Figure 2. Lifting structure for a two-component KLT. Conditional permutation included.

B. Implementation considerations

1) Side information: As the KLT, the POT requires the use of side information —usually the transform matrix, and the offset of each component so that it has zero mean— to indicate a specific inverse transform to the decoder. The amount of side information of the KLT is usually negligible if the image has a medium or large spatial size, yet, for images with small spatial size, the amount of side information of the KLT has an impact on the coding performance [21]. Contrarily, the POT requires a much smaller amount of side information, which is further reduced by transmitting only t as a half-precision IEEE 754 floating-point number, for each pairwise transform. Note that only t is required to be transmitted as p, q, and u can be directly derived from t (Eq. 2). As an example, without any side information quantization or coding, for an AVIRIS hyperspectral image of 224 components, the KLT would require at least 101 kilobytes of side information, whereas just 1340 bytes would suffice for the POT.

2) Line-based POT: With such a small amount of required side information, it is possible to apply the POT in a line by line basis, as shown in Fig. 3, where each line of an image is processed independently of the rest. As already processed input lines can be discarded, a line-based transform does not require buffering the whole image, substantially reducing the memory requirements.

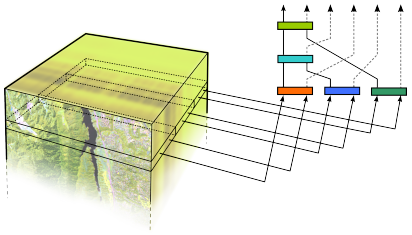

Figure 3. Example of a line-based application of a POT on a hyperspectral image with six components.

Moreover, most of the current hyperspectral sensors capture images over a fixed width window with a height of just one pixel, and use the motion of the sensor itself to provide the remaining spatial dimension of the image, specifically, either in pushbroom mode —capturing all the spectral bands of a line at once— or whiskbroom mode —capturing information in a Band Interleaved By Pixel (BIP) order [24]—. Both modes are particular cases of line-by-line image acquisition, and are well suited to the use of a POT transform in line-based processing, for instance in on-board applications.

A particular order within the pushbroom mode — Band Interleaved By Line (BIL) — is the most suitable to perform

a line-based POT, because a coder, in addition to being able to discard already processed lines, is also able to discard the already processed components of a line. When a POT is applied to a BIL-ordered image, where each component is read sequentially for each line, as soon as two consecutive components of a line are read, both can be transformed, and one of them flushed to the output, while the other follows to the higher levels of the structure, where it may also be transformed again. This process is illustrated in Fig. 4, where only a portion of two spectral components of a line is required to remain in memory. Contrarily, for a BIP order, due to the transform training stage, a complete line has to be buffered before the transform can be trained and then applied.

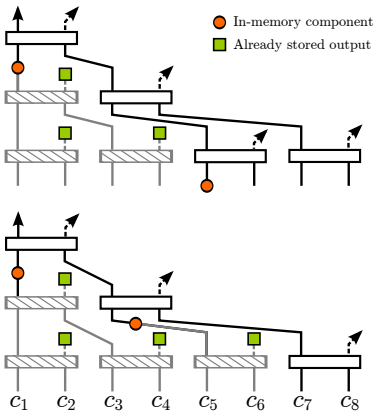

Figure 4. Internal state of an eight component transform when components are read sequentially. Internal state before (top), and after (bottom), the sixth component of the image (c_6) is read.

3) Covariance computation: Another aspect of the transform usage is the calculation of the covariance matrices, Σ_{X}, which amounts to one third of the forward transform cost, and can be optimized with knowledge of the eigenvalues of previous levels of transform. For each pairwise transform, the covariance of its output is:

$$\Sigma_{\mathrm{Y}} = \frac{1}{M}\mathrm{Y}\mathrm{Y}^T = Q^T\Sigma_{\mathrm{X}}Q = \Lambda.$$

Since, first level apart, pairwise transforms receive its inputs from other transforms outputs, the variance of an input component is already computed (in Λ from the other transform), and corresponds to the eigenvalue λ_1 associated with that component. As such, values a and d from Σ_{X} for transforms beyond the first level are already available, while b is not available because the two inputs have not been examined jointly before. Deriving a and d from previous transforms reduces the total cost of covariance matrix calculation by two thirds for those transforms, and one third globally.

4) Range expansion: When a POT is applied over an image, the numeric range of its values is increased because energy is accumulated on a few components. Knowing the exact range expansion is required, for example, to allocate correct register sizes.

The range expansion for each lossy two-component transform can be calculated as follows. From Eq. 1 and 2,

$$\begin{pmatrix} y_1 \\ y_2 \end{pmatrix} = \begin{pmatrix} \sqrt{1-t^2} & t \\ -t & \sqrt{1-t^2} \end{pmatrix} \begin{pmatrix} x_1 \\ x_2 \end{pmatrix},$$

and hence

$$peak_{y_1} = \max_{-1\le t\le 1} |\sqrt{1-t^2}x_1 + tx_2|.$$

Combining the peak values of both inputs as $peak_{in} = \max\{|x_1|, |x_2|\}$, yields a peak output value bounded by

$$peak_{out} \le peak_{in} \cdot \max_{-1\le t\le 1} \sqrt{1-t^2} + |t| = peak_{in}\sqrt{2}.$$

On the lossless case one has also to take into account the error introduced by the lifting structure (Fig. 2), which is bounded by [22, Eq. 19] to

$$||\mathbf{u}||_\infty \le \frac{2 + |w_3| + \max\{1 + |w_2|, |w_3| + |w_3 \cdot w_2 + 1|\}}{2}.$$

The peak values for $|w_2|$ and $|w_3|$ are, respectively, 1 and $1+\sqrt{2}$, hence

$$||\mathbf{u}||_\infty \le 3 + \frac{3\sqrt{2}}{2} < 6.$$

As the number of levels of an N-component POT is not greater than $l = \lceil log_2 N \rceil$, the range expansion of the whole transform is bounded by

$$peak_{out} < (peak_{in} + 6l)\sqrt{2}^l,$$

which corresponds to an increase of 5 bits in register size for a 256-component transform applied to 16bit data.

C. Analytical Evaluation

Having considered several implementation issues, this section reports an analysis of the proposed POT with respect to the following three inconveniences of classical KLT: computational cost, memory requirements, and component scalability. It will be shown that none of these three inconveniences remains in a POT.

1) Computational cost: The high computational cost of the KLT renders it unpractical and even unusable on many situations. As an example, costs to apply lossy forward and inverse transforms on a typical AVIRIS image for KLT, POT, and wavelets are given in Fig. 5. In this particular case, KLT cost is over 30 times higher than that of POT or wavelets, and POT cost is slightly lower than wavelets.

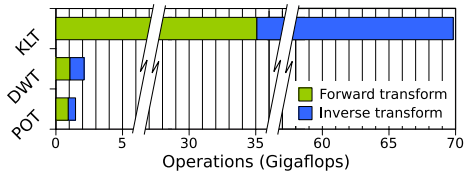

Figure 5. Cost comparison to apply lossy forward and inverse transforms to a common AVIRIS image of size $677 \times 512 \times 224$ ($x \times y \times z$).

In Table I, a detailed analysis of the transform costs is provided. Dominant terms are highlighted in the last two columns.

Table I
TRANSFORM APPLICATION AND REMOVAL COST (IN FLOPS). ρ IS THE COVARIANCE SUBSAMPLING FACTOR [4], n IS THE NUMBER OF SPECTRAL COMPONENTS, AND $m = xy$ IS THE NUMBER OF SPATIAL LOCATIONS OF THE ORIGINAL IMAGE. DOMINANT TERMS ARE DETERMINED ASSUMING $m \ggg n$ AND $\rho \simeq 0.01$. FOR WAVELET TRANSFORMS, l IS THE NUMBER OF LEVELS, AND COST IS EXACT IF $n = 2^l k, k \in \mathbb{N}$.

	Computational cost		Dominant terms	
Spectral transform	Forward	Inverse	Fwd.	Inv.
Full KLT lossy	$9n^3 + m((2+\rho)n^2 + (\rho+1)n + 4\rho)$	$2mn^2$	$2n^2m$	$2n^2m$
Full KLT lossless	$m((3+\rho)n^2 + (2+\rho)n + 4\rho - 3) + \frac{32}{3}n^3 + \frac{1}{2}n^2 - \frac{37}{6}n + 5$	$m(3n^2 + n - 3)$	$3n^2m$	$3n^2m$
POT lossy	$12mn + 21ny - 8m - 23y$	$7mn + 3ny - 6m - 3y$	$12nm$	$7nm$
POT lossless	$16mn + 26ny - 12m - 28y$	$11mn + 5ny - 10m - 5y$	$16nm$	$11nm$
Wavelet CDF 9/7 lossy	$\simeq m(14n\sum_{i=1}^{l} 2^{-i})$	$\simeq m(14n\sum_{i=1}^{l} 2^{-i})$	$14nm$	$14nm$
Wavelet CDF 5/3 lossless	$\simeq m(-3l + 9n\sum_{i=1}^{l} 2^{-i})$	$\simeq m(-3l + 9n\sum_{i=1}^{l} 2^{-i})$	$9nm$	$9nm$

The main difference among the dominant terms is the squared factor for the KLT, which substantially increases transform cost as the number of components increase. POT and wavelets transforms have an approximately linear cost in relation to components or spatial locations, and they mainly differ on a constant factor. In both forward and inverse modes, a lossy POT has a lower constant factor than a lossy CDF 9/7, while the opposite happens in the lossless case. Nonetheless, both POT and wavelets entail a very affordable cost.

2) Memory requirements: A transform with a low memory requirement can be used in memory constrained environments, and it often involves non-proportional memory requirements, allowing the coding of arbitrarily large images regardless of the available memory capability. KLT has a huge memory requirement, proportional to the whole image size, which is usually well over a hundred megabytes. Contrarily, due to the POT being able to operate in a line-based mode, POT requires a tiny amount of memory, which is often around a few kilobytes. Peak memory requirements for the KLT, the POT, and wavelets are reported in Table II, both when the image is fed to the transform in BIL order, and when it is fed in BIP order. Although the reported results for the POT and wavelets are both of acceptable magnitude, it is of interest to note the small amount of memory needed by wavelet transforms when data is in BIP mode, a direct consequence of wavelets not having a training stage, enabling them to start producing results as soon as all bands of one pixel are available.

Table II
APPROXIMATE PEAK MEMORY REQUIREMENTS, MEASURED IN NUMBER OF COEFFICIENTS. IN PARENTHESES, BYTES NEEDED WHEN $n = 224$, $y = 512$, $x = 677$, $l = 5$, AND COEFFICIENT BIT DEPTH IS 16 BPPPB.

Spectral transform	BIL	BIP
Full KLT	$n^2 + nm + n$ (148 MB)	$n^2 + nm + n$ (148 MB)
POT	$(1 + \log_2(n))x + 6$ (12 kB)	$xn + 6$ (296 kB)
Wavelet CDF 9/7	$6lx$ (40 kB)	$6l$ (60 bytes)
Wavelet CDF 5/3	$4lx$ (26 kB)	$4l$ (40 bytes)

3) Component scalability: In the context of multi-component image coding, a spectral transform provides component scalability if it allows to partially reverse the transform without needing to invert the full transform. A transform with component scalability allows for features such as region of interest retrieval, progressive decoding, and interactive transmission. In this case too, the KLT has a serious impairment, since even to recover only one component, the full transform has to be reversed. Table III reports the component scalability of the three compared spectral transforms. POT is the transform with better scalability, followed by wavelets —which have a poorer component scalability—, and, at a much larger distance, by KLT, that does not provide any scalability. To successfully take advantage of the transform scalability, it is important to pair the transform with a scalable coder, such as JPEG2000, which apart from the spectral transform and the Rate-Distortion (R-D) optimization stage does not have any additional band interdependency.

Table III
TRANSFORM SCALABILITY (IN COMPONENTS REQUIRED TO RECOVER ONE COMPONENT). n IS THE NUMBER OF SPECTRAL COMPONENTS. l IS THE NUMBER OF WAVELET LEVELS. REPORTED WAVELET SCALABILITY MAY BE REDUCED ON TRANSFORM EDGES DUE TO COEFFICIENT MIRRORING (UP TO A HALF).

Spectral transform	Dependent components	avg. (min. / max.) ($n = 224, l = 5$)
Full KLT lossy	n	224.0 (224/224)
Full KLT lossless	n	224.0 (224/224)
POT lossy	$\simeq 1 + \log_2(n)$	8.9 (8/9)
POT lossless	$\simeq 1 + \log_2(n)$	8.9 (8/9)
Wavelet CDF 9/7	$\simeq 7l - 2^{-l} - 1$	36.0 (32/38)
Wavelet CDF 5/3	$\simeq 3l - 2^{-l} - 1$	16.0 (11/17)

III. EXPERIMENTAL RESULTS

To evaluate the suitability of POT for hyperspectral image coding, extensive experimental tests have been performed, including classification-based experiments. In this section, results are reported and discussed.

Experiments have been conducted on a corpus composed of several images from AVIRIS [25] and Hyperion [26] sensors. Images obtained with an AVIRIS sensor have 224 spectral components covering wavelengths from 370 to 2500 nm. For the experiments with AVIRIS images, scenes with only the first 512 lines of each image have been used. The AVIRIS corpus includes images from various stages of the acquisition chain: uncalibrated images, radiance images, and reflectance images.

Hyperion images have a fixed width of 256 columns, a variable height, and 242 spectral components covering wavelengths from 357 to 2576 nm, from which only 198 components are calibrated. The Hyperion corpus includes uncalibrated images and radiance images. The Hyperion sensor has a 12 bpppb bitdepth, while the AVIRIS sensor has evolved over the years and some of its features have changed; in particular, bitdepth initially was 12 bpppb, and currently is 16 bpppb. After calibration, image bitdepth is 16 bpppb. Table IV provides full technical names and sizes for the images used. The described images can be obtained at [25], [27], [28].

Table IV
TECHNICAL NAMES FOR AVIRIS AND HYPERION IMAGES USED.

Image Name	Technical Name	Size ($x \times y \times z$)[1]
AVIRIS		
Cuprite	f970619t01p02_r02	$614 \times 2206 \times 224$
Jasper Ridge	f970403t01p02_r03	$614 \times 2586 \times 224$
Low Altitude	f960705t01p02_r05	$614 \times 3689 \times 224$
Lunar Lake	f970623t01p02_r07	$614 \times 1431 \times 224$
Moffett Field	f970620t01p02_r03	$614 \times 2031 \times 224$
Yellowstone (Sc K)	f060925t01p00_r12_sc$K$	$677 \times 512 \times 224$
Hawaii	f011020t01p03r05_sc01	$614 \times 512 \times 224$
Maine	f030828t01p00r05_sc10	$680 \times 512 \times 224$
Hyperion		
Coastal	EO1H0140342002050110PY	$256 \times 2905 \times 224$
Erta Ale	EO1H1680502010057110KF	$256 \times 3188 \times 242$
Lake Monona	EO1H0240302009166110PF	$256 \times 3177 \times 242$
Mt. St. Helens	EO1H0460282009231110KF	$256 \times 3243 \times 242$
Urban	EO1H0440342002212110PY	$256 \times 2905 \times 224$

A spectral transform is usually the first stage of the coding process; hence, to assess compression gains, a spectral transform has to be tested in conjunction with an image coder. Three coders have been selected for this purpose: JPEG2000 [29], 3d-TCE [1], and Ter [30], an improved version of the Consultative Committee for Space Data Systems (CCSDS) recommendation for Image Data Compression [31]. JPEG2000 is a standardized multipurpose image coding system, which provides good performance and is well suited for long term archival. 3d-TCE is an embedded tarp-based coder, with a performance similar to JPEG2000, but that differs from JPEG2000 in that it uses a different approach to provide probability estimates in the transformed domain. Ter, highly focused on satellite image compression, enhances the CCSDS recommendation with volumetric rate-distortion, quality scalability, and other features. All three coders are able to perform both lossy and Progressive Lossy-to-Lossless (PLL) encodings of volumetric images, although in this case, only 3d-TCE tries to exploit three-dimensional redundancy by using a volumetric probability context in addition to the spectral transform.

Implementations employed to perform the experiments are: Kakadu for JPEG2000 [32], QccPack for 3d-TCE [33], Ter for CCSDS-IDC [34], and our own open-source implementation of the KLT and the POT [35]. Coding systems are alternated to show that transform performance results are consistent regardless of the coding method used.

From the computational cost point of view, it has to be taken into account that a transform is one stage of the whole coding process of a coding system, and that other stages may present higher computational costs and memory requirements depending on the combination of transform and coder selected. Particularly, to achieve a low memory cost, the coder implementation has to be able to code in parallel and in a line-based mode all the bands of an image (such as Kakadu software does). Implementation difficulty is increased by coding the image in line-based mode, mainly because multiple transforms are applied at once and the state of each one has to be maintained. Note also, that image coders that only perform pure lossless codings of hyperspectral images usually have lower costs than a full transform coder with PLL capabilities.

Both for lossy and for lossless modes, the proposed POT spectral transform is evaluated in comparison to the KLT and to a Discrete Wavelet Transform (DWT) (Cohen-Daubechies-Feauveau (CDF) 9/7 for lossy coding and CDF 5/3 for PLL, with 5 levels). No spatial clustering is applied to the KLT, and side information for all transforms is coded with zlib [36].

There are several variations of a three-dimensional DWT (e.g., a pyramid wavelet decomposition, or a hybrid 1D+2D wavelet decomposition such as the one used), and multiple DWT-based coders. The use of a hybrid 1D+2D wavelet in combination with a transform coder like JPEG2000 is the recommended approach for this scenario in recent literature [37], [38], [4], [39], as being the one that provides best performance.

The rest of this section is organized as follows: first, an issue with pushbroom sensors is addressed, next, the results for lossy coding are discussed, then, PLL results are reported, followed by pure lossless experiments, and, finally, some classification-based results are disclosed.

A. Pushbroom sensors

Due to the nature of pushbroom sensors (i.e., those sensors that capture all the spectral bands of a line at once by a bidimensional sensor array), vertical streaking artifacts might appear, as happens for Hyperion sensor. These artifacts, shown in Fig. 6, have its cause on the use of an array of sensors and the slight variations among each of them. These artifacts are mostly removed by the calibration process [2], but on uncalibrated images, streaking artifacts have a severe impact on coding performance because they hinder the detection of redundancy in adjacent locations.

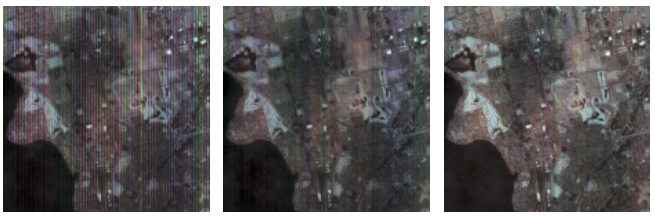

(a) Uncalibrated (b) Preprocessed (c) Calibrated

Figure 6. Pushbroom sensor artifacts on a region of the Hyperion image Lake Monona before calibration (a), with a simple preprocessing (b), and after calibration (c).

To limit the impact of these artifacts, a very simple preprocessing stage can be applied to uncalibrated images from the

[1]Uncalibrated Yellowstone images are 680 columns wide, and uncalibrated Hyperion images have one line less that the calibrated ones.

pushbroom sensor Hyperion. The preprocessing is a reversible process based on shifting the values of image columns to smooth differences with their neighbors, and is undone after decompression just as if it were an additional transform. First, shifting offsets are obtained by

$$\delta_{i,k} = \frac{1}{32}\sum_{j=0}^{31} \underset{|m|\leq 4}{\text{median}} \left(I_{w(i+m,0,x-1),j.k}\right),$$

where $I_{i,j,k}$ is the value of original image at band k, row j, column i, and x is the image width.

Only the first 32 lines are used to obtain shifting offsets. Afterwards, each image location, as it is retrieved, is modified according to the previous offset by

$$\hat{I}_{i,j,k} = w(I_{i,j,k} - [\delta_{i,k}], -2^{15}, 2^{15} - 1)$$

The function w warps any integer value to the interval $[a, b]$ with symmetric reflection around a if $i < a$ or around b if $i > b$, i.e.,

$$w(i, a, b) = b - |b - a - (i - a \bmod 2(b - a))|.$$

B. Lossy coding

Fig. 7 reports the R-D evolution of the different spectral transforms, KLT, POT, and wavelet CDF 9/7. The plots provide a relation between quality, measured in Signal-to-Noise Ratio (SNR), and bitrate, measured in bits per pixel per band (bpppb). In this case, SNR is defined as $\text{SNR} = 10\log_{10}(\sigma^2/\text{MSE})$, where σ^2 is the variance of the original image. A steady quality evolution can be observed for all transforms in both examples, with KLT obtaining the best performance, followed by POT, and wavelet CDF 9/7 producing the worst coding results.

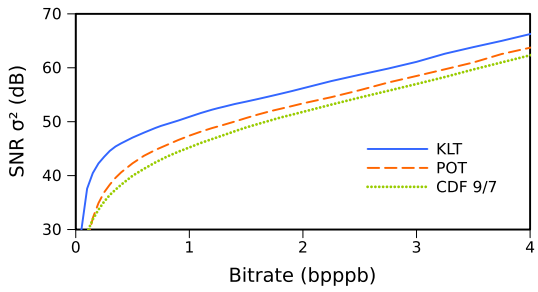

(a) AVIRIS Moffett Field Radiance coded with JPEG2000

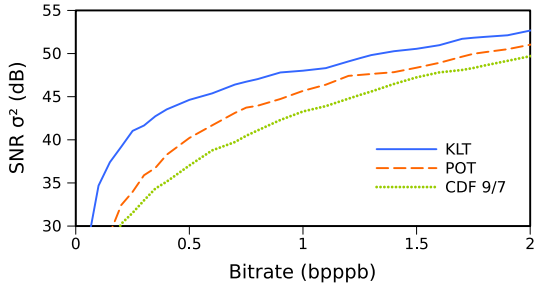

(b) AVIRIS Low Altitude Radiance coded with Ter

Figure 7. R-D performance comparison among the three spectral transforms.

Coding performance for uncalibrated images from the Hyperion sensor, reported in Fig. 8, varies depending on whether a preprocessing is applied to remove streaking artifacts or not. The transform most affected by streaking artifacts seems to be the POT, but all three transforms are heavily affected by the artifacts. From now on, the preprocessing is included in all codings of uncalibrated Hyperion images, and the operation is reversed on decodings.

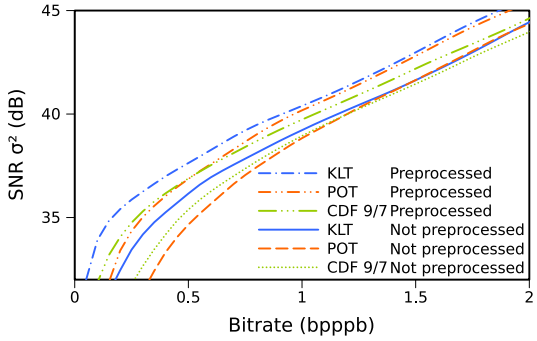

Figure 8. Effects of pushbroom preprocessing. Image is Hyperion Lake Monona. Coding system is JPEG2000.

Fig. 9 reports comparisons of coding performance between radiance and uncalibrated images, and Fig. 10 between radiance and reflectance images, when JPEG2000 is used as coding system. From the first comparison, it seems that wavelets suffer a noticeable penalization on uncalibrated images from the AVIRIS sensor, and on calibrated images from the Hyperion sensor.

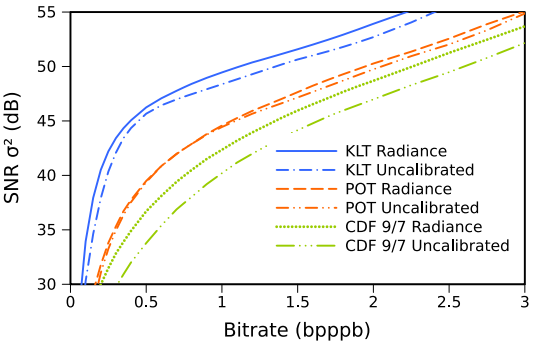

(a) AVIRIS Yellowstone

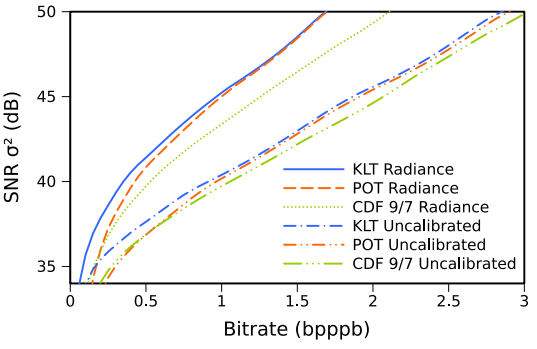

(b) Hyperion Lake Monona

Figure 9. Comparison of transform performance between uncalibrated and radiance images. Coding system is JPEG2000.

Table V shows a detailed comparison for lossy coding between POT and wavelet CDF 9/7 in relation to the coding

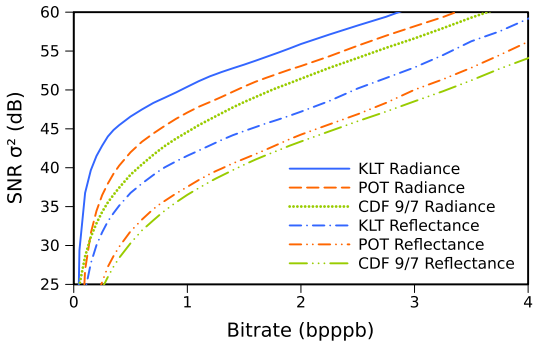

Figure 10. Comparison of transform performance between a radiance and reflectance image. Image is AVIRIS Jasper Ridge. Coding system is JPEG2000.

results of the KLT. Results show a moderate performance penalty for POT, and a higher performance penalty for the wavelet. In the reported experiments, the performance decrease of the wavelet CDF 9/7 spectral transform in the average case is always higher than the performance decrease of the POT, with POT yielding results between 1 to 5 dB higher, except for uncalibrated Hyperion images, where gains are more modest perhaps because of the smaller difference between the KLT and DWT.

An important remark is that, for lossy coding of hyperspectral images, the most appropriate distortion measure would often be how well posterior processing and exploitation tasks perform on imagery lossy coded, specially for uncalibrated images, where a calibration process is always applied. This is not a trivial assessment at all, as many different processing and exploitation tasks can be applied, and each often requires particular datasets (e.g., ground truth for a supervised land cover classifier, or models on sensor response for the echo cancellation in the calibration of Hyperion images). See below, in Section III-E, two examples of these particular evaluations. If the posterior processing or exploitation task is known, small corrections over a lossy image might be coded as side information to improve performance, as in [40], or a more general approach can be followed by combining a lossy transform coder with a quantized coding of the residual image in a near-lossless approach [41], [42].

As shown in Fig. 11, at very low bitrates —less than 0.5 bpppb— some artifacts appear on the POT because of its line-based application. Artifacts are barely perceptible unless a strong sharpening filter is applied, and disappear as bitrate increases. The low affectation by blocking artifacts of the POT might be explained by the small size of each transform partition (i.e., one line), which enables a smooth transition between them. If it were of interest to reduce these artifacts, the variable t of each two-component transform and the zero-mean offsets could be smoothed by a regularizing filter with the values of adjacent lines.

C. Progressive lossy-to-lossless coding

Results are also similar when PLL coding performance is evaluated, as reported in Fig. 12. Note that, at very high bitrates, a lossless POT produces better results than a lossless

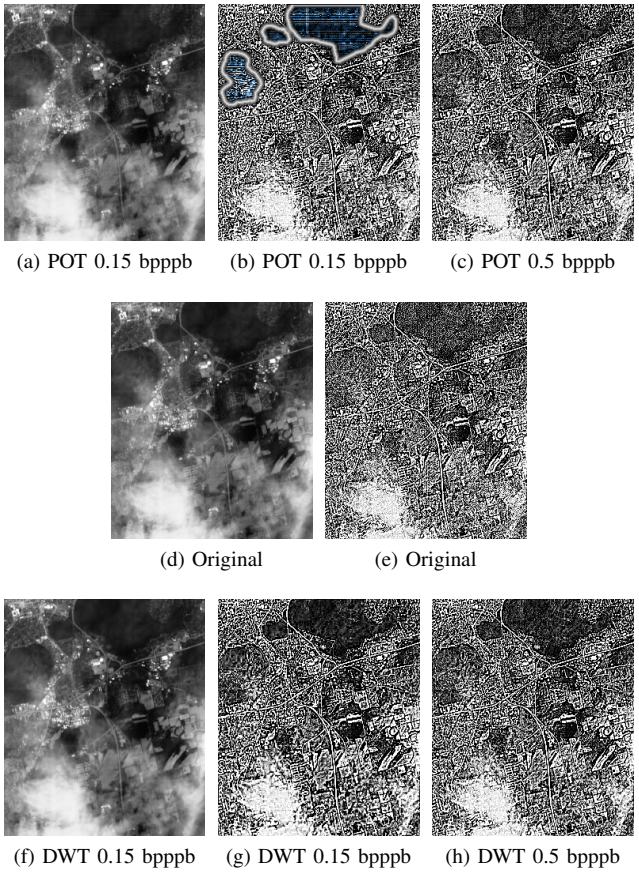

(a) POT 0.15 bpppb (b) POT 0.15 bpppb (c) POT 0.5 bpppb

(d) Original (e) Original

(f) DWT 0.15 bpppb (g) DWT 0.15 bpppb (h) DWT 0.5 bpppb

Figure 11. Blocking artifacts at very low bitrates. Component 20 of Hyperion image Lake Monona coded with JPEG2000. Images in (b), (c), (e), (g) and (h) had a sharpening filter applied.

RKLT, due to the smaller number of lifting steps of the former, which causes smaller quantization errors before lossless regime is achieved. For uncalibrated Hyperion images, the RKLT performance drop is more noticeable and starts at lower bitrates (even if images are not preprocessed for pushbroom artifacts). Results for TCE yield similar performance gains.

D. Pure lossless coding

Table VI reports bitrates required for lossless coding, and compares them with bitrates needed by pure lossless methods. As happened for PLL, the same relative performance is maintained among the three spectral transforms, KLT, POT, and wavelets, except for Hyperion radiance images, where the line-by-line adaption of the POT may be outweighing its less general decorrelation ability, and renders POT performance superior to KLT. On Hyperion uncalibrated images, while on average the relative order is also maintained, the difference between the three transforms is not significant.

With regard to an analysis among radiance, reflectance, and uncalibrated images, it seems that radiance images are the ones where compression is more effective, producing smaller file sizes. When pure lossless methods are taken into account in the comparison, an interesting remark is that a clear division exists between the old 12 bpppb AVIRIS images from 1996/97, and the newer 16 bpppb Yellowstone scenes from 2006. For

Table V
SNR DIFFERENCE (IN DB) BETWEEN KLT, POT, AND WAVELET CDF 9/7. KLT IS USED AS REFERENCE, AND BITRATE IS SAMPLED AT $b = 0.1k$, $k = 2, 3, \ldots, 20$ AND MEASURED IN BPPPB. IMAGES ARE CODED WITH JPEG2000.

	POT			Wavelet CDF 9/7		
	avg.	min.	max.	avg.	min.	max.
AVIRIS Cuprite Radiance	−0.81	(−1.32 / −0.68)		−3.32	(−5.24 / −2.54)	
AVIRIS Jasper Ridge Radiance	−3.41	(−6.02 / −2.53)		−5.96	(−8.70 / −4.46)	
AVIRIS Low Altitude Radiance	−2.90	(−5.95 / −1.80)		−6.14	(−9.45 / −3.92)	
AVIRIS Lunar Lake Radiance	−0.77	(−1.39 / −0.64)		−2.75	(−4.41 / −2.08)	
AVIRIS Moffett Field Radiance	−3.56	(−6.28 / −2.62)		−5.82	(−8.62 / −4.38)	
AVIRIS Yellowstone (Sc 0) Radiance	−4.74	(−7.18 / −3.43)		−7.26	(−10.62 / −5.21)	
AVIRIS Yellowstone (Sc 11) Radiance	−4.02	(−6.86 / −2.96)		−5.50	(−8.94 / −3.80)	
AVIRIS Yellowstone (Sc 18) Radiance	−6.03	(−8.73 / −4.21)		−7.95	(−11.24 / −5.54)	
Hyperion Coastal Radiance	−0.47	(−1.69 / −0.18)		−2.85	(−3.47 / −2.46)	
Hyperion Erta Ale Radiance	−0.19	(−1.01 / 0.00)		−2.36	(−2.98 / −1.96)	
Hyperion Lake Monona Radiance	−0.38	(−1.89 / −0.03)		−1.98	(−2.60 / −1.61)	
Hyperion Mt. St. Helens Radiance	−0.51	(−1.79 / −0.20)		−3.12	(−3.63 / −2.77)	
Hyperion Urban Radiance	−0.87	(−2.53 / −0.44)		−3.88	(−4.87 / −3.45)	
AVIRIS Cuprite Reflectance	−2.17	(−4.71 / −1.25)		−7.89	(−12.46 / −4.91)	
AVIRIS Jasper Ridge Reflectance	−3.80	(−5.63 / −2.79)		−5.18	(−7.40 / −3.84)	
AVIRIS Lunar Lake Reflectance	−1.54	(−3.72 / −0.92)		−4.91	(−9.12 / −3.22)	
AVIRIS Moffett Field Reflectance	−4.03	(−5.66 / −2.90)		−7.03	(−10.70 / −4.72)	
AVIRIS Hawaii Uncalibrated	−1.88	(−3.30 / −1.38)		−4.14	(−8.83 / −3.03)	
AVIRIS Maine Uncalibrated	−2.15	(−5.27 / −1.40)		−4.83	(−10.99 / −2.97)	
AVIRIS Yellowstone (Sc 0) Uncalibrated	−3.93	(−5.90 / −2.72)		−8.40	(−12.36 / −5.72)	
AVIRIS Yellowstone (Sc 11) Uncalibrated	−1.03	(−1.30 / −0.64)		−4.10	(−5.86 / −2.69)	
AVIRIS Yellowstone (Sc 18) Uncalibrated	−3.48	(−4.41 / −2.43)		−7.39	(−9.70 / −4.95)	
Hyperion Erta Ale Uncalibrated	−0.23	(−1.31 / +0.02)		−0.96	(−1.40 / −0.77)	
Hyperion Lake Monona Uncalibrated	−0.47	(−2.00 / −0.15)		−0.83	(−1.35 / −0.63)	
Hyperion Mt. St. Helens Uncalibrated	−0.72	(−2.22 / −0.31)		−1.68	(−2.86 / −1.39)	

radiance images, on the older images, two pure lossless methods, LAIS-QLUT (LQLUT) [43] and TSP-W2 [44], exploit artifacts introduced in the calibration process [44], yielding better performances, whereas, the combination of RKLT and JPEG2000 generally outperforms pure lossless methods on the newer Yellowstone scenes. On these new AVIRIS radiance images, POT has a severe penalization, yet, it provides better performance than wavelet CDF 5/3. For uncalibrated images, the pure lossless method FL [45] yields similar results as a combination of RKLT and JPEG2000, where the latter provides PLL capabilities at a higher computational cost.

E. Classification-based experiments

An additional set of experiments measures POT performance using classification-based metrics, i.e., it measures how classifiers are affected by the distortion introduced by a coding system. The classifiers used are k-Means for clustering (with 20 classes and Eulerian distance) [48] and Reed Xiaoli (RX) for anomaly detection (with a 2% threshold) [49]. An RX detector identifies locations that are different from the background by using the Mahalanobis distance to find outliers (see [50] for a review on its use on hyperspectral images). Both methods are unsupervised classifiers widely used on remote-sensing imagery. Results are reported in Preservation of Classification (POC) units, a percentage of how many spatial locations stay in the same class if coding distortion is added to the process.

In Fig. 13, results for k-Means [48] on the AVIRIS Moffett Field are presented. In this case, the wavelet has a slightly worse performance than POT, and results saturate quality-wise between 2 and 3 bpppb.

Fig. 14 reports results for a RX detector [49] on the AVIRIS Lunar Lake. In this case, results are more unstable, especially for the KLT, which seems to introduce distortion more detrimental to the classifier, perhaps because the Mahalanobis distance is also calculated in a KLT-transformed version of the image (i.e., another KLT not related to the one used for coding). Although POT composes several KLT, it does not produce such artifacts. Apart from the RX instability with a KLT, results are consistent with the previous ones, showing POT providing better results than wavelets.

IV. CONCLUSIONS

In this paper, a new spectral transform is proposed for the removal of spectral redundancy in hyperspectral image coders. KLT and wavelets are the most common spectral transforms, but KLT has four inconveniences that impair its practical use, and wavelets provide a lower coding performance.

The proposed POT is based on the composition of multiple two-component instances of the KLT. The use of such composition allows for substantial benefits in computational cost, component scalability, memory requirements, and implementation difficulty.

A detailed analysis of the proposed transform is presented, comparing POT with a full KLT and with wavelets, and describing the different properties of the transform. Analysis indicates that memory requirements and implementation difficulty are the issues where our contribution is more substantial. Due to the small amount of side information needed by POT, a line-based approach is amenable, which requires four orders of magnitude less memory than a full KLT. In addition, due to the use of two-component KLT, the diagonalizing of the covariance matrix can be greatly simplified, from a

Table VI
LOSSLESS BITRATE FOR KLT, POT, AND CDF 5/3 WITH JPEG2000 (IN BPPPB). FIVE PURE LOSSLESS METHODS ARE ALSO INCLUDED AS REFERENCE: FAST-LOSSLESS (FL) [45], LAIS-QLUT (LQLUT) [43], TSP-W2 [44], KSP [46], AND A1 FROM [47]. FOR THESE RESULTS, AVIRIS RADIANCE IMAGES HAVE BEEN USED IN ITS FULL HEIGHT.

	RKLT	POT	CDF 5/3	FL	LQLUT	TSP-W2	KSP	A1
AVIRIS Cuprite Radiance	4.91	5.03	5.36	4.91	4.48	3.77	4.88	5.50
AVIRIS Jasper Ridge Radiance	4.86	5.32	5.60	4.95	4.70	4.08	4.96	5.60
AVIRIS Low Altitude Radiance	5.16	5.51	5.85	5.26	5.00	4.31	—	—
AVIRIS Lunar Lake Radiance	4.91	5.01	5.29	4.91	4.53	3.81	4.90	5.51
AVIRIS Moffett Field Radiance	4.91	5.29	5.60	4.99	4.79	4.12	4.92	5.64
AVIRIS Yellowstone (Sc 0) Radiance	3.86	4.44	4.73	3.96	4.48	3.99	—	4.81
AVIRIS Yellowstone (Sc 11) Radiance	3.62	4.09	4.24	3.63	4.02	3.67	—	4.41
AVIRIS Yellowstone (Sc 18) Radiance	3.78	4.50	4.69	3.94	4.48	3.97	—	4.77
Hyperion Coastal Radiance	5.50	5.18	5.79	—	—	—	—	—
Hyperion Erta Ale Radiance	5.66	5.30	5.89	—	—	—	—	—
Hyperion Lake Monona Radiance	5.81	5.49	6.02	—	—	—	—	—
Hyperion Mt. St. Helens Radiance	5.67	5.38	6.02	—	—	—	—	—
Hyperion Urban Radiance Radiance	5.76	5.49	6.19	—	—	—	—	—
AVIRIS Cuprite Reflectance	6.01	6.14	6.75	—	—	—	—	—
AVIRIS Jasper Ridge Reflectance	5.96	6.32	6.61	—	—	—	—	—
AVIRIS Lunar Lake Reflectance	6.04	6.10	6.60	—	—	—	—	—
AVIRIS Moffett Field Reflectance	6.10	6.47	6.86	—	—	—	—	—
AVIRIS Hawaii Uncalibrated	2.85	2.98	3.26	2.64	3.05	2.62	2.84	3.49
AVIRIS Maine Uncalibrated	2.97	3.07	3.41	2.72	3.19	2.74	2.90	3.65
AVIRIS Yellowstone (Sc 0) Uncalibrated	6.07	6.63	7.13	6.23	6.78	6.27	6.34	6.92
AVIRIS Yellowstone (Sc 11) Uncalibrated	6.10	6.27	6.60	5.86	6.30	5.88	—	6.53
AVIRIS Yellowstone (Sc 18) Uncalibrated	6.24	6.72	7.12	6.32	6.82	6.32	—	6.92
Hyperion Erta Ale Uncalibrated	4.26	4.30	4.34	—	—	—	—	—
Hyperion Lake Monona Uncalibrated	4.37	4.45	4.44	—	—	—	—	—
Hyperion Mt. St. Helens Uncalibrated	4.27	4.37	4.44	—	—	—	—	—

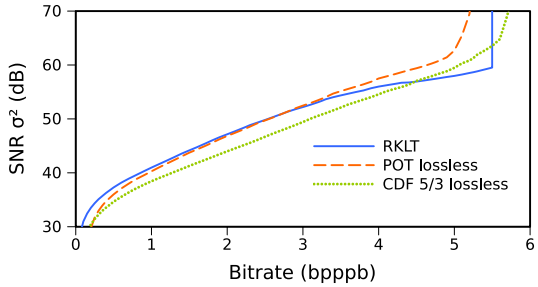

(a) Hyperion Coastal Radiance coded with JPEG2000

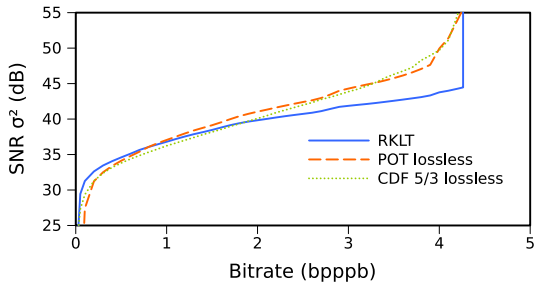

(b) Hyperion Erta Ale Uncalibrated coded with JPEG2000

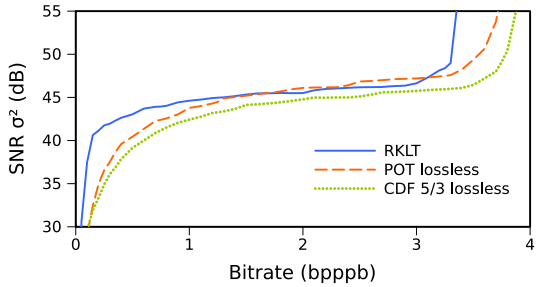

(c) AVIRIS Yellowstone Radiance coded with TCE

Figure 12. R-D performance comparison among the three spectral transforms for PLL

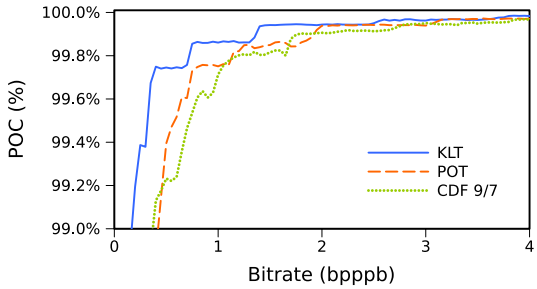

Figure 13. Performance of k-Means clustering for the AVIRIS Moffett Field. Coding system is JPEG2000.

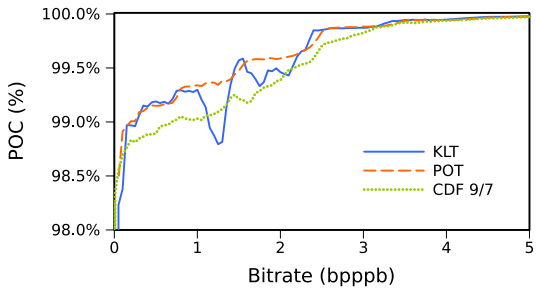

Figure 14. Performance of RX anomaly detection for the AVIRIS Lunar Lake. Coding system is JPEG2000.

complex iterative process, to a direct calculation. Moreover, the proposed transform also has a computational cost with a linear complexity in relation to the number of spectral components, as opposed to KLT, which has a quadratic complexity (i.e., POT cost is forty-five times smaller than KLT for AVIRIS images). Finally, POT also provides a good component scalability, better than that provided by wavelets, and much better than KLT.

Extensive experimental results are conducted for AVIRIS and Hyperion images, and for three different image coding systems, JPEG2000, TCE, and Ter, an improved version of the CCSDS IDC recommendation. Results consistently report that the proposed POT spectral transform has better performance than wavelets, although it does not reach the coding performance of a full KLT. Results are reported for radiance, reflectance and uncalibrated images, for lossy, progressive lossy-to-lossless, and pure lossless coding, and for classification-based metrics. Generally, for all images tested, and on all experimental results, the proposed transform outperforms wavelets.

In conclusion, the proposed POT is a transform that might be a good replacement for wavelets as spectral decorrelator of hyperspectral images in all the scenarios where a KLT is not a feasible option, or simply where the extra coding performance of the KLT is not worth its associated burdens.

ACKNOWLEDGMENT

The authors would like to thank the anonymous reviewers for their valuable comments, and Aaron Kiely for providing Hyperion images.

REFERENCES

[1] J. Zhang, J. E. Fowler, and G. Liu, "Lossy-to-lossless compression of hyperspectral imagery using three-dimensional TCE and an integer KLT," *IEEE Geosci. Remote Sens. Lett.*, vol. 5, pp. 814–818, Oct. 2008.

[2] J. Pearlman, P. Barry, C. Segal, J. Shepanski, D. Beiso, and S. Carman, "Hyperion, a space-based imaging spectrometer," *IEEE Trans. Geosci. Remote Sens.*, vol. 41, no. 6, pp. 1160–1173, Jun. 2003.

[3] N. Ahmed, T. Natarajan, and K. Rao, "Discrete cosine transfom," *IEEE Trans. Comput.*, vol. C-23, no. 1, pp. 90–93, Jan. 1974.

[4] B. Penna, T. Tillo, E. Magli, and G. Olmo, "Transform coding techniques for lossy hyperspectral data compression," *IEEE Trans. Geosci. Remote Sens.*, vol. 45, no. 5, pp. 1408–1421, May 2007.

[5] L. Lan and I. Reed, "Fast approximate Karhunen-Loeve transform (AKLT) with applications to digital image-coding," *Elsevier Visual Commun. and Image Process. 93*, vol. 2094, pp. 444–455, 1993.

[6] A. Pirooz and I. Reed, "A new approximate Karhunen-Loeve transform for data compression," *Conference Record of the Thirty-Second Asilomar Conference on Signals, Systems and Computers*, vol. 1-2, pp. 1471–1475, 1998.

[7] I. R. Greenshields and J. A. Rosiene, "A fast wavelet-based Karhunen-Loeve transform," *Pattern Recognition*, vol. 31, no. 7, pp. 839–845, Jul. 1998.

[8] M. Cagnazzo, L. Cicala, G. Poggi, and L. Verdoliva, "Low-complexity compression of multispectral images based on classified transform coding," *Elsevier Signal Processing-Image Communication*, vol. 21, no. 10, pp. 850–861, 2006.

[9] C. Thiebaut, E. Christophe, D. Lebedeff, and C. Latry, "CNES studies of on-board compression for multispectral and hyperspectral images," in *Satellite Data Compression, Communications, and Archiving III*, R. W. Heymann, B. Huang, and I. Gladkova, Eds., vol. 6683, no. 1. SPIE, 2007, p. 668305.

[10] L. Wang, J. Wu, L. Jiao, and G. Shi, "3D medical image compression based on multiplierless low-complexity RKLT and shape-adaptive wavelet transform," *ICIP 2009. Proceedings of 2009 International Conference on Image Processing*, pp. 2521–2524, Nov. 2009.

[11] ——, "Lossy-to-lossless hyperspectral image compression based on multiplierless reversible integer TDLT/KLT," *IEEE Geosci. Remote Sens. Lett.*, vol. 6, no. 3, pp. 587–591, July 2009.

[12] I. P. Akam Bita, M. Barret, and D.-T. Pham, "On optimal orthogonal transforms at high bit-rates using only second order statistics in multicomponent image coding with JPEG2000," *Elsevier Signal Processing*, vol. 90, no. 3, pp. 753 – 758, 2010.

[13] ——, "On optimal transforms in lossy compression of multicomponent images with JPEG2000," *Elsevier Signal Processing*, vol. 90, no. 3, pp. 759–773, 2010.

[14] M. Barret, J.-L. Gutzwiller, I. P. Akam Bita, and F. Dalla Vedova, "Lossy hyperspectral images coding with exogenous quasi optimal transforms," in *Data Compression Conf. 2009 (DCC 2009)*. IEEE Press, Mar. 2009, pp. 411–419.

[15] I. P. Akam Bita, M. Barret, F. Dalla Vedova, and J.-L. Gutzwiller, "Lossy compression of MERIS superspectral images with exogenous quasi optimal coding transforms," in *Satellite Data Compression, Communication, and Processing V*, B. Huang, A. J. Plaza, and R. Vitulli, Eds., vol. 7455, no. 1. SPIE, 2009, p. 74550U.

[16] Y. Wongsawat, "Lossless compression for 3-D MRI data using reversible KLT," *Int'l Conf. on Audio, Language and Image Processing, 2008. (ICALIP 2008).*, pp. 1560–1564, July 2008.

[17] I. Blanes and J. Serra-Sagristà, "Clustered reversible-KLT for progressive lossy-to-lossless 3d image coding," in *Data Compression Conf. 2009 (DCC 2009)*. IEEE Press, Mar. 2009, pp. 233–242.

[18] ——, "Cost and scalability improvements to the Karhunen-Loêve transform for remote-sensing image coding," *IEEE Trans. Geosci. Remote Sens.*, 2010, in press.

[19] J. A. Saghri and S. Schroeder, "An adaptive two-stage KLT scheme for spectral decorrelation in hyperspectral bandwidth compression," *Proc. SPIE*, vol. 7443, p. 744313, 2009.

[20] J. A. Saghri, S. Schroeder, and A. G. Tescher, "Adaptive two-stage Karhunen-Loeve-transform scheme for spectral decorrelation in hyperspectral bandwidth compression," *SPIE Optical Engineering*, vol. 49, p. 057001, May 2010.

[21] Q. Du, W. Zhu, H. Yang, and J. E. Fowler, "Segmented principal component analysis for parallel compression of hyperspectral imagery," *IEEE Geosci. Remote Sens. Lett.*, vol. 6, no. 4, pp. 713–717, Oct. 2009.

[22] P. W. Hao and Q. Y. Shi, "Matrix factorizations for reversible integer mapping," *IEEE Trans. Signal Process.*, vol. 49, no. 10, pp. 2314–2324, 2001.

[23] L. Galli and S. Salzo, "Lossless hyperspectral compression using KLT," *IEEE Int'l Geosci. and Remote Sens. Symp. Proc. (IGARSS 2004)*, vol. 1-7, pp. 313–316, 2004.

[24] F. Kruse, J. Boardman, and J. Huntington, "Comparison of airborne hyperspectral data and EO-1 Hyperion for mineral mapping," *IEEE Trans. Geosci. Remote Sens.*, vol. 41, no. 6, pp. 1388–1400, June 2003.

[25] Jet Propulsion Laboratory, NASA, "Airborne Visible InfraRed Imaging Spectrometer website," http://aviris.jpl.nasa.gov/html/aviris.overview.html.

[26] U.S. Geological Survey and NASA, "Earth Observing 1, Hyperion website," http://eo1.usgs.gov/hyperion.php.

[27] Jet Propulsion Laboratory, NASA, "Hyperspectral image compression website," http://compression.jpl.nasa.gov/hyperspectral/.

[28] U.S. Geological Survey, "Earth explorer," http://earthexplorer.usgs.gov.

[29] D. Taubman and M. Marcellin, *JPEG2000: Image Compression Fundamentals, Standards, and Practice*. Kluwer International Series in Engineering and Computer Science, 2002, vol. 642.

[30] F. Garcia-Vilchez and J. Serra-Sagristà, "Extending the CCSDS Recommendation for Image Data Compression for Remote Sensing Scenarios," *IEEE Trans. Geosci. Remote Sens.*, vol. 47, no. 10, pp. 3431 –3445, 2009.

[31] Consultative Committee for Space Data Systems, "Image Data Compression," Blue Book, CCSDS 122.0-B-1, Nov. 2005.

[32] D. Taubman, "Kakadu software," http://www.kakadusoftware.com/, 2000.

[33] J. Fowler, "QccPack: An open-source software library for quantization, compression, and coding," in *Applications of Digital Image Processing XXIII*, A. Tescher, Ed., vol. 4115, San Diego, CA, USA, Aug. 2000, pp. 294–301.

[34] Group on Interactive Coding of Images, "TER software; Open Source CCSDS-122-B-1 implementation and extension." http://www.gici.uab.cat/TER, http://ter.sourceforge.net/, June 2008.

[35] Group on Interactive Coding of Images, "Spectral transform software," http://gici.uab.cat/, 2010.

[36] P. Deutsch and J.-L. Gailly, "ZLIB compressed data format specification version," May 1996. [Online]. Available: http://www.gzip.org/zlib/rfc1950.pdf

[37] B. Penna, T. Tillo, E. Magli, and G. Olmo, "A new low complexity KLT for lossy hyperspectral data compression," *IGARSS 2006. IEEE International Conference on Geoscience and Remote Sensing Symposium, 2006.*, pp. 3525–3528, 2006.

[38] ——, "Progressive 3-D coding of hyperspectral images based on JPEG2000," *IEEE Geosci. Remote Sens. Lett.*, vol. 3, no. 1, pp. 125–129, Jan. 2006.

[39] J. E. Fowler and J. T. Rucker, *Hyperspectral Data Exploitation: Theory and Applications*. Hoboken, NJ, USA: John Wiley & Sons Inc., 2007, ch. "3D wavelet-Based Compression of Hyperspectral Imager", pp. 379–407.

[40] B. Penna, T. Tillo, E. Magli, and G. Olmo, "Hyperspectral image compression employing a model of anomalous pixels," *IEEE Geosci. Remote Sens. Lett.*, vol. 4, no. 4, pp. 664–668, 2007.

[41] A. Lucero, S. Cabrera, E. J. Vidal, and A. Aguirre, "Evaluating residual coding with JPEG2000 for L-infinity driven hyperspectral image compression," *Satellite Data Compression, Communications, and Archiving*, vol. 5889, no. 1, pp. 12–23, 2005. [Online]. Available: http://link.aip.org/link/?PSI/5889/588903/1

[42] G. Carvajal, B. Penna, and E. Magli, "Unified lossy and near-lossless hyperspectral image compression based on JPEG 2000," *IEEE Geosci. Remote Sens. Lett.*, vol. 5, no. 4, pp. 593–597, Oct. 2008.

[43] J. Mielikainen and P. Toivanen, "Lossless compression of hyperspectral images using a quantized index to lookup tables," *IEEE Geosci. Remote Sens. Lett.*, vol. 5, no. 3, pp. 474–478, July 2008.

[44] A. Kiely and M. Klimesh, "Exploiting calibration-induced artifacts in lossless compression of hyperspectral imagery," *IEEE Trans. Geosci. Remote Sens.*, vol. 47, no. 8, pp. 2672–2678, Aug. 2009.

[45] M. Klimesh, "Low-complexity adaptive lossless compression of hyperspectral imagery," *Proc. SPIE*, pp. 63 000N.1–63 000N.9, Sept. 2006.

[46] E. Magli, "Multiband lossless compression of hyperspectral images," *IEEE Trans. Geosci. Remote Sens.*, vol. 47, no. 4, pp. 1168–1178, Apr. 2009.

[47] A. Abrardo, M. Barni, E. Magli, and F. Nencini, "Error-resilient and low-complexity onboard lossless compression of hyperspectral images by means of distributed source coding," *IEEE Trans. Geosci. Remote Sens.*, vol. 48, no. 4, pp. 1892–1904, Apr. 2010.

[48] J. B. MacQueen, "Some methods for classification and analysis of multivariate observations," in *Proc. 5th Berkeley Symp. Math. Statistics and Probability*, L. M. L. Cam and J. Neyman, Eds., vol. 1. University of California Press, 1967, pp. 281–297.

[49] I. Reed and X. Yu, "Adaptive multiple-band CFAR detection of an optical pattern with unknown spectral distribution," *IEEE Trans. Acoust., Speech, Signal Process.*, vol. 38, no. 10, pp. 1760–1770, Oct. 1990.

[50] C.-I. Chang and S.-S. Chiang, "Anomaly detection and classification for hyperspectral imagery," *IEEE Trans. Geosci. Remote Sens.*, vol. 40, no. 6, pp. 1314–1325, Jun. 2002.